Tellus
SERIES B
CHEMICAL
AND PHYSICAL
METEOROLOGY
PUBLISHED BY THE INTERNATIONAL METEOROLOGICAL INSTITUTE IN STOCKHOLM

Tellus (2010), 62B, 242–258
Printed in Singapore. All rights reserved

TELLUS

A downscaling scheme for atmospheric variables to drive soil–vegetation–atmosphere transfer models

By A. SCHOMBURG[1]*, V. VENEMA[1], R. LINDAU[1], F. AMENT[2] and C. SIMMER[1],
[1]*Meteorological Institute University of Bonn, Germany*; [2]*ZMAW, University of Hamburg, Germany*

(Manuscript received 2 December 2009; in final form 15 June 2010)

ABSTRACT

For driving soil–vegetation–transfer models or hydrological models, high-resolution atmospheric forcing data is needed. For most applications the resolution of atmospheric model output is too coarse. To avoid biases due to the non-linear processes, a downscaling system should predict the unresolved variability of the atmospheric forcing. For this purpose we derived a disaggregation system consisting of three steps: (1) a bi-quadratic spline-interpolation of the low-resolution data, (2) a so-called 'deterministic' part, based on statistical rules between high-resolution surface variables and the desired atmospheric near-surface variables and (3) an autoregressive noise-generation step. The disaggregation system has been developed and tested based on high-resolution model output (400 m horizontal grid spacing). A novel automatic search-algorithm has been developed for deriving the deterministic downscaling rules of step 2. When applied to the atmospheric variables of the lowest layer of the atmospheric COSMO-model, the disaggregation is able to adequately reconstruct the reference fields. Applying downscaling step 1 and 2, root mean square errors are decreased. Step 3 finally leads to a close match of the subgrid variability and temporal autocorrelation with the reference fields. The scheme can be applied to the output of atmospheric models, both for stand-alone offline simulations, and a fully coupled model system.

1. Introduction

The Earth's surface is characterized by heterogeneity extending from microscopic to global scales. Heterogeneity is found in land use, orography, soil texture and additionally caused by spatial variability in atmospheric forcing, such as different microclimates or precipitation patterns. Most processes in the soil and at the interface between soil and atmosphere are highly non-linear. Examples are threshold-dependent processes such as runoff production, snow melt and stomata control; or the turbulent exchange coefficients, which are non-linear functions of the near-surface atmospheric stability. For these reasons modelling of the exchange processes either needs to be performed at high resolutions, or has to account for this subgrid heterogeneity in some other way. The use of averaged state variables or parameters instead leads to systematic errors (e.g. Schlünzen and Katzfey, 2003).

An increasing number of atmospheric models comprise already some kind of subgrid scale surface heterogeneity representation. A common concept is the so-called mosaic or explicit subgrid approach by Avissar and Pielke (1989). The soil–vegetation–atmosphere transfer (SVAT) module is run on a higher horizontal resolution than the respective atmospheric model, which is feasible because current soil modules are considerably less computationally expensive than their atmospheric counterpart. The high-resolution turbulent fluxes at the interface are averaged to the coarser (atmospheric) scale before passing them over to the atmospheric model. Usually a constant atmospheric forcing for all subpixels belonging to one atmospheric column is assumed to drive the SVAT model. However, especially over heterogeneous land surfaces also the lower part of the atmospheric boundary layer is heterogeneous. Furthermore, this atmospheric heterogeneity to some degree induces (or reduces) surface heterogeneity. Thus, a spatially distributed atmospheric forcing is advisable.

An explicit distribution of atmospheric forcing in combination with the mosaic approach was first tested by Seth and Giorgi (1994). The authors disaggregated temperature, humidity, convective precipitation and clouds to the high surface resolution. Temperature and humidity were downscaled proportional to either soil temperature and soil moisture anomalies, or, in a second comparison, orographic height anomalies. The method was tested for a stand-alone version of the biosphere–atmosphere transfer scheme (BATS, Dickinson et al., 1993) and evaluated with respect to surface fluxes and hydrology (soil moisture and runoff). The horizontal resolution in their study was still rather

*Corresponding author.
e-mail: aschomburg@uni-bonn.de
DOI: 10.1111/j.1600-0889.2010.00466.x

coarse (3.0° atmospheric resolution with 0.5° mosaic resolution), and simulations were carried over a time period of 20 yr. The authors found that due to the downscaling of atmospheric variables the heat fluxes changed by up to 15% and the runoff up to 33%. Arola (1999) extended this technique by applying stability corrected logarithmic profiles to compute the local wind speed, temperature and humidity at the reference level for the flux calculations, which lead to further improvements in the modelling of the sensible heat flux.

Giorgi et al. (2003) adopted this idea by employing a mosaic in a regional climate model with 60 km grid spacing over the alpine region, where the heterogeneity is particularly large. They employed a disaggregation based on topographic height; the temperature was downscaled using a moist adiabatic lapse rate multiplied with the elevation anomaly. Humidity was disaggregated accordingly, keeping the relative humidity constant for all subpixels, thus adjusting the specific humidity according to the temperature adjustment. Convective precipitation was distributed over one (randomly chosen) third of the subpixels. Grid scale precipitation, radiation fluxes and wind speed were not disaggregated. Using this system in simulations running 11 months led to an improved small-scale structure and an overall better simulation of the near-surface temperature over complex terrain. This produced a more realistic snow cover and (via feedback processes) also a better simulation of the water and energy cycle, especially during winter and in spring during and after snow melt.

The cited studies show that considerable improvements can be achieved by taking variable atmospheric forcing into account for driving small-scale soil models. All studies addressed, however, only scales of the order of 100 km (i.e. the climate scale). Moreover, small-scale variability was introduced to a subset of the atmospheric forcing variables only.

Hydrological models usually operate at even higher resolutions than SVAT models, because water flow must be simulated down to the scales of individual creeks for runoff prediction. Thus downscaling of atmospheric driving fields becomes even more important (see e.g. Seuffert et al., 2002). A good review of effects, which can result from neglected rainfall variability, is given by Singh (1997). In a study by Naden (1992) spatial variability was introduced implicitly into a hydrograph for estimating flood risks by applying weights to the network-width function, which describes the spatial distribution of channels in a catchment. A more physical approach, based on a disaggregation of all forcing variables, is presented by a study by Boé et al. (2007). They forced a hydrological model with differently downscaled atmospheric data and compared the resulting river discharges. Downscaling was performed dynamically including a bias correction and statistically based on weather typing and conditional resampling using large-scale variables as predictors. They found the statistical approach being more efficient in reproducing the temporal and spatial autocorrelations.

Our approach addresses the scale gap between high-resolution surface models and atmospheric models running on a coarser grid. It has been developed and tested on much smaller scales than the aforementioned studies. The novelty of our approach is the explicit reconstruction of the small-scale statistics, that is, the subgrid scale variance. The reproduction of the correct variance is especially important if the downscaled variables are used as input data to model non-linear processes. Venema et al. (2009), for example, demonstrate this for non-linear radiative transfer through clouds. We follow a statistical approach guided by physical considerations. High-resolution (400 m) coupled model simulations are used to generate a data set, from which the downscaling rules are derived.

The COnsortium for Small-scale Modelling model (COSMO), for which we developed our scheme, is a mesoscale weather-forecast model and regional climate model (see Section 2 for a brief model description and the chosen setup). The atmospheric disaggregation introduced here represents a further advancement of the work by Ament and Simmer (2006), who implemented and tested the mosaic approach in the COSMO model. Our concept can, however, be easily adapted to generate input for other SVAT or hydrological models that need high-resolution atmospheric forcing input.

Our downscaling system for atmospheric variables comprises three steps. In a first step we apply a bi-quadratic spline interpolation, which conserves the coarse pixel value as a mean (see Section 3.1). In the second step high-resolution surface information is used to exploit relationships between surface and atmospheric near-surface variables (Section 3.2). A novel automatic rule-search algorithm has been set up, to find relationships, which might act only under certain atmospheric conditions. In the final step autoregressive noise is added in order to replenish the variance in the high-resolution runs (Section 3.3). The application of this disaggregation system to the different variables is shown in Section 4, a summary and final conclusions are given in Section 5.

2. Model and data

2.1. Setup of high-resolution model runs

The training and validation of the disaggregation system is based on model output of COSMO model runs with 400 m horizontal grid spacing and by comparing this high-resolution model output to averaged 2.8 km values. We carried out simulations for a number of cases on a small model domain ($168 \times 168\,\mathrm{km}^2$). For operational applications, longer model runs, or larger model domains, such a high resolution is still too expensive to compute.

The COSMO-model is a limited-area non-hydrostatic modelling system (Steppeler et al., 2003), which is employed as operational weather prediction model by several European weather services on different resolutions. The model can also be run as a regional climate model (Böhm et al., 2006; Bachner et al.,

2008). The model configuration used for this work is based on the so-called COSMO-DE model version (Baldauf et al., 2009), which is operated on a 2.8 km horizontal grid by the German Meteorological Service (Deutscher Wetterdienst, DWD) on a model domain centred over Germany. Hence, with our disaggregation approach, it is possible to run the COSMO-model on 2.8 km atmospheric grid spacing and the soil module on 400 m, with the downscaling scheme as interface between these two scales. In this setup the model has 50 vertical layers, with decreasing thickness from top to bottom, with the lowest layer above the surface having a thickness of 20 m. Subgrid scale processes are calculated as functions of the model variables using parametrization schemes, they are described in detail in Doms et al. (2007).

The 400 m resolution runs require an appropriate setup and the preparation of a set of external parameters.

Our model domain is centred over the catchments of the two small rivers Rur and Erft, which is the main investigation area of the Transregional Collaborative Research Centre 32, in which framework this work has been carried out. The timestep was reduced from 25 s in the standard 2.8 km resolution model runs to 4 s in our 400 m simulations, to obey the Courant–Friedrich–Levy (CFL) stability criterion for the dynamic processes. Radiation computations are carried out for every column at a temporal resolution of 3 minutes, in order to keep track of the clouds. Turbulence is parametrized by a simple Prandtl/Kolmogorov approach. This approach is based on a first-order closure assumption, where the coefficients are parametrized based on stability functions (Smagorinsky, 1963) and a length scale, which is a function of the grid spacing to take the numerical resolution into account. The gradients in three-dimensional space are considered; the horizontal turbulent exchange coefficients are, however, simply obtained by scaling the vertical coefficients to the horizontal grid spacing. This scheme has been developed specifically for very high resolutions of the magnitude of 100 m.

The lower boundary condition of the atmospheric model is specified by the multilayer soil and vegetation model TERRA (Doms et al., 2007). Coupling of soil and atmosphere takes place via precipitation and formation of dew and rime as sources of water, and evaporation, transpiration and runoff as sinks. The heat exchange is given by the net radiation budget, the ground heat flux and the turbulent heat flux.

The information on the state of the Earth's surface is contained in an external parameter set. Orographic height information is taken from the Shuttle Radar Topography Mission (SRTM, Farr et al., 2007) data, whereas the CORINE data set (EEA, 2000) has been used for land use characteristics. Each pixel is attributed to one of 44 land use classes. Vegetation characteristics such as plant cover and leaf area index are then determined from these classes by means of look-up-tables. The merging of data sets from North Rhine-Westphalia (IS BK50) and Rhineland-Palatinate (BÜK200) was necessary to determine the soil texture distribution of the region. Different soiltype classes in the two data sets were mapped onto the eight soil-categories used in the COSMO-model. For the western parts of the model domain, covering parts of the Netherlands, Belgium and Luxembourg, no small-scale soil information was available, thus here we had to adopt the coarse information of the FAO/UNESCO Soil Map of the World from 1974 with a resolution of 5 arcmin, which is operationally used by DWD. All thermal and hydraulic soil parameters are derived from soil texture classes by look-up-tables, which contain values for the different parameters for each of the eight soil classes. These values have been compiled from literature.

COSMO-DE analyses with 2.8 km horizontal grid spacing are used for initialization and boundary forcing. This implies a factor of seven in resolution for the driving model with respect to the nested model, which is at the upper limit for nesting, thus a broad relaxation zone at the lateral boundaries of 20 km (50 grid boxes) has been chosen. Except for soil moisture, the relatively smooth initialization state, which results from an interpolation of the 2.8 km analysis, becomes heterogeneous by grid-scale variability after a few time steps. For soil moisture histogram matching according to the soil type has been implemented as an intermediate step to create more realistic variability: soil moisture values belonging to a certain soiltype from the coarse soiltype field are matched to the new, small-scale soiltype distribution.

2.2. Data

2.2.1. Training data. Eight high-resolution coupled model runs for different weather situations have been carried out for our high-resolution database (Table 1) at the basis of which the downscaling scheme is developed. The first two hours of each model run were discarded in order to remove spin-up effects. Days with calm, clear-sky weather, as well as days with unstable convective situations and also days with strong synoptic forcing were chosen to cover a wide range of weather situations. Cases with homogeneous stratiform cloud cover are included, as well as cases with fast moving clouds under stormy conditions.

2.2.2. Validation data: case studies. The downscaling scheme has been validated on three days with very different weather types (see also Table 1): May 12, 2008 was characterized by very calm weather conditions. Central Europe was under the influence of a stable high-pressure system for several days. Precipitation was absent and only very sparse cloud cover was observed. During May 15, 2008, Central Europe was under the influence of several low-pressure systems situated over the Atlantic Ocean and northern Europe. The high-pressure system was weakening and moved to southeastern Europe. Under these rather unstable conditions the model domain was almost completely covered by convective clouds during the whole day, including showers and thunderstorms. On July 16, 2008 a low-pressure system over the Northern Atlantic influenced the weather conditions in Central Europe, with a cold front crossing northern Germany during the

Table 1. Overview of simulated days including prevailing weather situation

Date	Weather situation
Training	
27 August, 2007	Changing cloud cover, no precipitation
14/15 October, 2007	Clear sky
3 March, 2008	Strong winds, variable clouds and precipitation
1/2 May, 2008	Convective clouds and precipitation
9/10 May, 2008	Clear sky
8 June, 2008	Convective clouds and precipitation
21 July, 2008	Synoptically driven stratiform rainfall
28 August, 2008	Cloudy, some rain
Validation	
12 May, 2008	Calm, only sparse cloud cover
15 May, 2008	Convective clouds, showers and thunderstorms
16 July, 2008	Stratiform rain

day. The strong synoptical forcing lead to stratiform rainfall and homogeneous cloud cover over the model domain.

3. The downscaling approach

The downscaling scheme is designed to recover as good as possible from the averaged coarse field (2.8 km grid spacing, for an example temperature field see Fig. 1, left-hand panel) the original fine-scale field (400 m grid spacing, Fig. 1, middle panel). This is equivalent to predicting the anomalies (Fig. 1, right-hand panel) based on the coarse atmosphere resolution and the high-resolution land surface information. Downscaling is necessary for those atmospheric variables which are needed as input for a SVAT model or a hydrological model (see Table 2). These are the variables of the lowest atmospheric model layer, which has a thickness of 20 m in the case of the COSMO model. Hence the variables are either assumed to be representative for 10 m above ground (the middle of the layer) or directly at the surface.

Our disaggregation system consists of three steps, which can be applied either individually or subsequently one after the other, depending on the variable and the application under consideration. The first step interpolates the coarse resolution to the fine resolution by bi-quadratic splines in x- and y-direction, while conserving mean and gradients of the coarse field. The second step exploits empirical relationships between atmospheric variables and surface variables using the available high-resolution

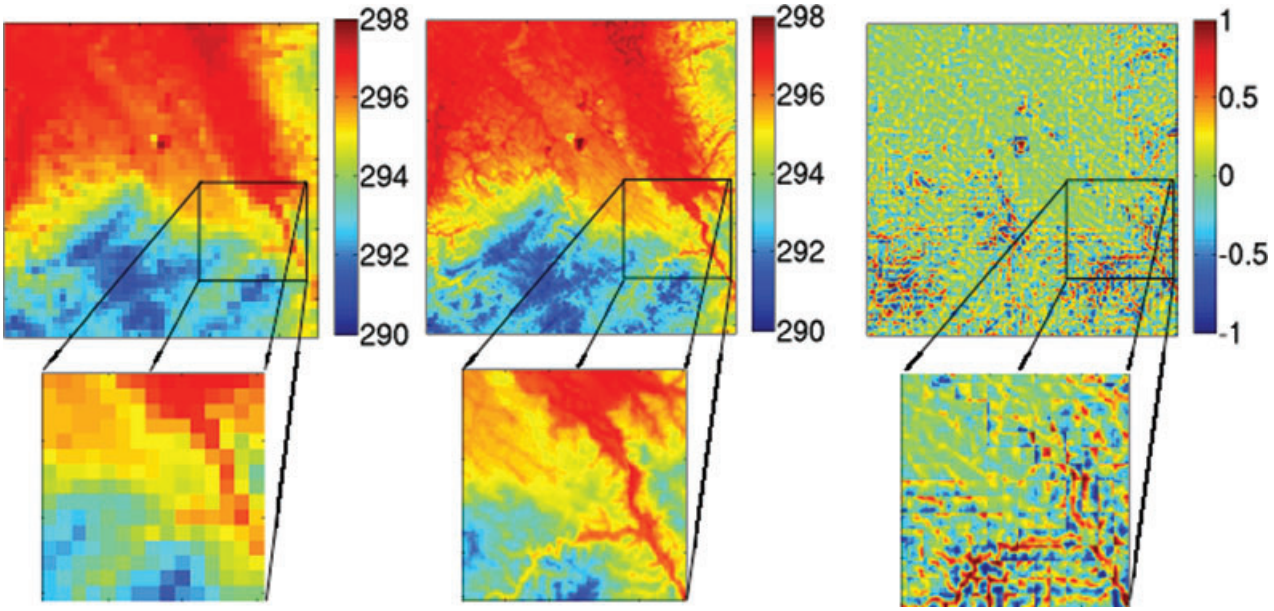

Fig. 1. Temperature at the lowest atmospheric model level on May 9, 2008 at 12:00 UTC in Kelvin at 2.8 km resolution (left-hand panel), 400 m resolution (middle panel) and the anomalies, i.e. the differences between both (right-hand panel).

Table 2. Downscaled variables

Variable	Abbreviation
Temperature at lowest model layer	T
Specific humidity at lowest model layer	QV
Wind speed at lowest model layer	FF
Short-wave net radiation flux at surface	S_{net}
Long-wave net radiation flux at surface	L_{net}
Precipitation (rain, snow, graupel)	$PREC$
Surface pressure	PS

surface information ('deterministic' downscaling rules). The third step adds the still missing high-resolution variability by adding noise. Thus downscaling steps 1 and 2 reconstruct the high-resolution fields as accurately as possible, and step 3 replenishes the mostly too low small-scale variability up to the variability of the high-resolution simulations. Since step 3 will usually increase again the error, a decision between low errors (apply only downscaling step 1 and 2) or a realistic small-scale variance (apply also step 3) has to be made first. The three steps are explained in detail in the following.

3.1. Step 1: Spline interpolation

The average-conserving bi-quadratic spline equation used in the first step

$$f(x, y) = a_1 + a_2 x + a_3 y + a_4 x^2 + a_5 y^2 \tag{1}$$

requires five unknown coefficients for every coarse pixel. Thus five constraints have to be formulated. Four constraints are provided by the derivatives of eq. (1) at the edges between the coarse pixels, which are set to be equal to the derivative of the coarse field perpendicular to the edges. The conservation of the mean value serves as the fifth constraint.

3.2. Step 2: Deterministic downscaling rules

The second step tries to recover the difference between the spline interpolated field and the original high-resolution field with deterministic rules. For these rules the high-resolution surface information is used as predictor based on linear regression.

Some variables can be downscaled by directly exploiting known physical relationships. By this means the surface pressure anomaly can be downscaled by using the relief height anomaly Δz in the hydrostatic equation

$$\Delta p = -\rho g \Delta z. \tag{2}$$

The assumption of a homogeneous constant air density of $1.19\,\text{kg}\,\text{m}^{-3}$ gives the best results.

The shortwave net radiation at the surface can be split up into

$$S_{\text{net}} = S_{\text{dir}}\downarrow + S_{\text{dif}}\downarrow - S_{\text{dif}}\uparrow \tag{3}$$

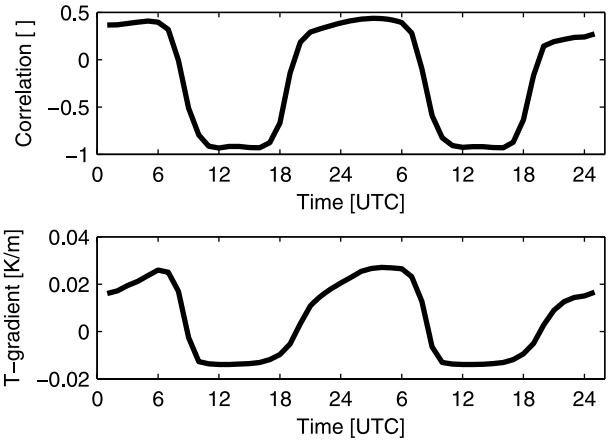

Fig. 2. Top panel: correlations between temperature anomalies in 10 m and orographic anomalies with respect to the coarse pixel scale of 2.8 km for 9 May 2008, a clear sky radiation day. Bottom panel: mean coarse scale vertical temperature gradient of the lowest four model layers.

with $S_{\text{dir}}\downarrow$ the incoming direct radiation from the sun, $S_{\text{dif}}\downarrow$ the diffuse downwelling radiation and $S_{\text{dif}}\uparrow$ the reflected diffuse upwelling radiation. The downscaled diffuse upwelling radiation can be obtained from the high-resolution surface albedo for direct and diffuse light, α_{dir} and α_{dif}, via

$$S_{\text{dif}}\uparrow = \alpha_{\text{dir}} S_{\text{dir}}\downarrow + \alpha_{\text{dif}} S_{\text{dif}}\downarrow . \tag{4}$$

The downwelling direct and diffuse radiation are not correlated with any surface variables. Both have little subgrid heterogeneity in cloud free cases (the average subgrid scale standard deviation is $2\,\text{W}\,\text{m}^{-2}$), while in cloudy situations their subgrid scale variability relates to cloud cover variability on the subgrid scale (the average subgrid scale standard deviation is $39\,\text{W}\,\text{m}^{-2}$). Thus in rather homogeneous cloudfree conditions the short-wave net radiation can be disaggregated with near perfect correlation because all subgrid variability is associated with surface (albedo) variability. Under cloudy conditions the variability has to be induced by stochastical methods (in step 3).

For the remaining five variables the situation is less intuitive because no direct relationship to surface characteristics exists. Thus, the high-resolution database was statistically evaluated for possible correlations between atmospheric and surface variables. Usually such correlations depend on the prevailing weather conditions. Figure 2 depicts the spatially averaged correlation between the temperature anomalies of the lowest atmospheric model layer and the topographic height anomalies (both with respect to the 2.8 km scale) for a clear sky day. Correlations are close to minus one during the day, as one would expect for a well-mixed boundary layer. The stratification leads to a simple decrease of temperature with topographic height, which can be exploited for the disaggregation of the high-resolution atmospheric near-surface temperature anomalies. During

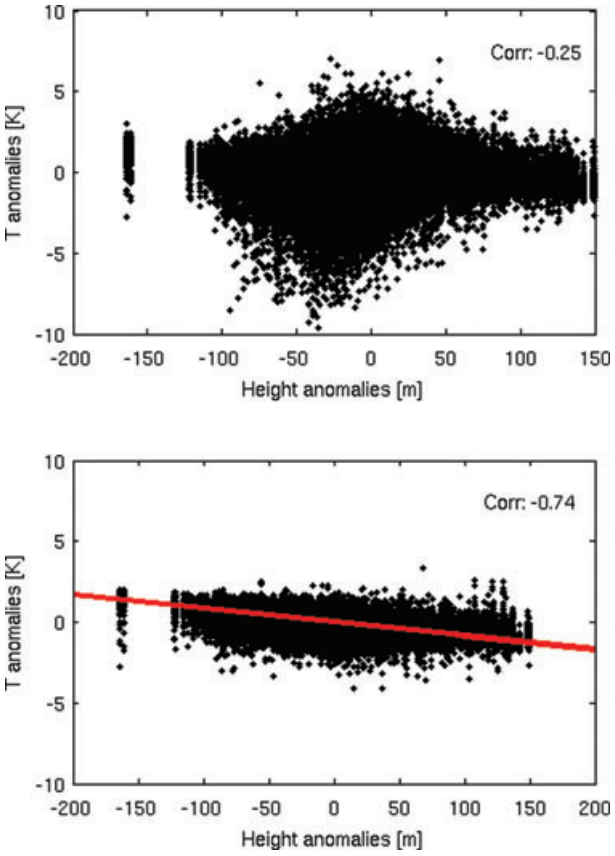

Fig. 3. Scatterplot of temperature anomalies versus orographic height anomalies with respect to the coarse pixel scale of 2.8 km. Top panel: all cases and bottom panel: only where the coarse temperature gradient of the lowest 105 m is lower than a threshold of 0.0057 K m^{-1}, with a linear fit.

clear-sky nights, however, when outgoing long-wave radiation leads to strong cooling of the ground, no or only a slightly positive correlation between temperature and elevation exists. Nighttime inversions and complex valley circulations destroy any usable statistical predictions. Thus prior to the use of the orographic high-resolution surface information as predictor for near surface temperatures, the temperature gradient of the lower atmosphere is computed and a decision made, based on its closeness to adiabatic stratification (see Fig. 2, bottom panel). For illustration the correlations without and with application of the temperature gradient as indicator are shown as scatter-plots in Figure 3. The statistical correlation between temperature and relief anomalies is very low for the complete database (Fig. 3, top panel); using the coarse-resolution temperature gradient as pre-selection criterion, however, a strong negative correlation exists (Fig. 3, bottom panel).

To find the most suitable predictors, indicators and thresholds, an automatic rule detection system has been developed. In this system the correlations between all possible predictors and the desired downscaled variables are calculated, based on indicators, which might allow or disallow the rule. The corresponding indicator thresholds are varied between the minimum and maximum value found in the database for each possible indicator variable in 30 steps. For 5 predictants, 16 possible predictors, 24 possible indicators, (see Table A1 in the Appendix for a list of all provided predictors and indicators), 30 indicator-range intervals, and the whole procedure performed two times (testing for situations where the indicator is larger or smaller than the threshold, respectively), a total of $5 \times 16 \times 24 \times 30 \times 2 = 115\,200$ correlations were computed. Only those rules are selected, which led to correlation coefficients above 0.7, that is, an explained variance of at least 50%. The final selection of a rule requires in addition, that the rule is applicable to at least 10% of the data.

Table A2 in the Appendix contains all rules detected by this automatic search system. If several indicators were found describing very similar situations, only the indicator applicable to the larger part of the data set is chosen. If more than one predictor is found for the desired variable, we tested its usefulness by a stepwise regression. As a final step for each of the downscaled variables the coefficients needed for a linear regression between downscaling variable and predictors have been computed.

For the near surface temperature several rules have been found, indicating that this variable is closely related to relief height or temperature gradient multiplied with relief height, with the coarse temperature gradient as indicator. In the end only the rule using orographic information in situations indicated by the temperature gradient of the lowest 105 m was taken as a rule, because it covered the largest part of the database (64%); using other predictors did not give substantial additional skill.

For specific humidity and wind speed no useful correlations with surface quantities have been found. Setting the desired correlation in the automatic search system to a lower value, that is, 0.5 (instead of 0.7 as before), we found correlations between near surface humidity *QV* and surface humidity *QVS* of 0.51 for 12% of the cases, detectable by the humidity gradient of the lowest two atmospheric layers. We discarded this rule for the current setup due to the low correlation.

With the same criterion also a relationship between wind speed *FF* and sensible heat flux was found; this relationship was discarded, however, because of the dependency of the sensible heat flux on wind speed. Also averaging the near surface and the surface quantities over an hour did not lead to usable correlations for wind speed or specific humidity. The fields of *QV* and *FF* at the lowest atmospheric layer contain many transient small-scale organized wave-like structures (not shown), indicating that these two variables are strongly dynamically driven, and thus determined by very small-scale dynamical processes. Thus, simple statistical relationship rules with surface variables are not able to reconstruct this variability. A small cross-correlation between wind speed and specific humidity of 0.27 exists, indicating that both are partly driven by the same dynamical circulations.

Table 3. Deterministic rules with the respective regression coefficients, correlations achieved and amount of data covered

Downscaling variable	Predictor	Constraint	Regression coefficient	Correlation	Data coverage
T	H	$Tgr105 < 0.0058$	$-0.0084\,\mathrm{Km}^{-1}$	0.74	64%
L_{net}	T_g	$L_{\mathrm{net}} < -82.5$	$-3.878\,\mathrm{W\,m}^{-2}\,\mathrm{K}^{-1}$	0.74	36%
PS	H	None	$-11.694\,\mathrm{Pa\,m}^{-1}$	1.0	100%

The net long-wave radiation L_{net} can be split up, into downward $L\downarrow$ and upward fluxes $L\uparrow$ according to

$$L_{\mathrm{net}} = L\downarrow - L\uparrow = L\downarrow - \left(\alpha_{\mathrm{IR}} L\downarrow + (1-\alpha_{\mathrm{IR}})\sigma T_g^4\right) \tag{5}$$

with α_{IR} the infrared albedo, σ the Stefan–Boltzmann constant and T_g the temperature of the emitting surface. We found that the ground temperature can be used to disaggregate the long-wave net radiation when the cloud cover is below 43% or the long-wave net radiation L_{net} is less than $-82.5\ \mathrm{W\,m}^{-2}$. Both indicators cover about the same situations. In cloudy cases the long-wave downwelling radiation anomalies are mainly determined by clouds and less by the emitted radiation from the surface, while in cloud-free situations the long-wave emission from the surface is the only source of heterogeneity.

As expected no rules have been found for precipitation. In Table 3 the regression coefficients, correlation achieved and data coverage for the rules found by the automatic rule detection system are listed. The regression coefficients are based on the same database as was used for the rule detection system (see Table 1).

3.3. Step 3: Noise generation

Except for surface pressure the downscaling steps 1 and 2 alone do not reproduce all small-scale variability contained in the simulated high-resolution fields. The full variance is, however, important when modelling the non-linear processes at the surface based on the downscaled variables. Lower variabilities can lead to biases in the computed fluxes when averaged over larger spatial and temporal scales. To avoid these biases, the yet unresolved variance is added as noise, at the expense of a higher error at the smallest scale. This third step is applied after carrying out the first two downscaling steps, or, for the variables for which no deterministic relationship can be found, directly after step 1.

3.3.1. Estimating the small-scale variance. We first assess the magnitude of the missing small-scale variability. To this end, a stepwise multiple linear regression system has been developed, which estimates the small-scale standard deviation based on the coarse-scale standard deviation of the surrounding 3×3 coarse pixels and other atmospheric variables, which serve as a measure for the atmospheric conditions. For each variable variance different predictors have been chosen by stepwise regression (Table 4). The exact regression equations are given in the appendix.

Table 4. Predictors for estimating the standard deviation (*SD*) at the small scale

Downscaling variable	Predictors
T	$Tgr25$, 3×3 coarse *SD*, *PS*
QV	3×3 coarse *SD*
FF	3×3 coarse *SD*, *PS*
S_{net}	3×3 coarse *SD*
L_{net}	3×3 coarse *SD*, subgrid *SD* of QVS

For variables for which downscaling step 2 has been applied, the variance generated by step 2 is subtracted from the estimated value from the regression to add only the still missing variance. If this difference is less than zero, no noise is added.

3.3.2. Algorithm for noise generation. The noise is modelled based on an autoregressive process, to account for its temporally correlated nature

$$x_{\mathrm{new}} = \phi x_{\mathrm{old}} + \epsilon, \tag{6}$$

where ϵ is a Gaussian noise term. The correlated noise has a zero mean value, because we reconstruct only the anomalies. To compute the intermediary autoregression noise term x_{new} with a standard deviation of unity, the standard deviation of ϵ is computed according to

$$\sigma_\epsilon = \sqrt{1-\phi^2}. \tag{7}$$

The autoregression coefficient ϕ is obtained by carrying out one or several model runs with high-resolution temporal output, and computing the autocorrelation for the desired variable and time lag. The coarse model at 2.8 km grid spacing (for the atmosphere) has a time step of 25 s, and the respective lag-1 autocorrelations ϕ were found to lie between 0.92 for the short-wave radiation and 0.97 for the specific humidity. The final noise field, which is added to the coarse field, is then obtained by

$$x_{\mathrm{noise}} = \sigma_{\mathrm{miss}} x_{\mathrm{new}}, \tag{8}$$

where σ_{miss} is the missing standard deviation estimated before. Spatial correlations are ignored in this step, in contrast to the first two steps. Addition of noise including the correct spatial correlations is planned for a future extension of the scheme.

For all the downscaling steps the coarse mean of the grid cell is conserved by subtracting the difference between the coarse value and the mean of the downscaled values, ensuring the conservation of energy and mass. In very rare cases negative values of wind speed, short-wave radiation or precipitation result from the statistical downscaling which should not be used to force a soil model or a hydrological model. Thus negative values are set to zero. The mean value of the coarse pixel is then conserved by multiplying the subgrid-pixel values by the fraction of the coarse means before and after setting these pixels to zero.

3.3.3. Special case: Precipitation. The downscaling of precipitation is treated as a special case, because additive noise would lead to many negative precipitation values and because Gaussian noise does not model the distribution of the anomalies well. The precipitation noise-generation algorithm consists of three steps. First, autoregressive Gaussian noise g is generated, similar to the other parameters. This noise is then transformed into the following distribution, setting values below a threshold to zero and transforming the other values by a power law

$$t = e^{[a*(g+b)]}. \tag{9}$$

The noise values t are subsequently multiplied by the coarse mean precipitation. The constants, that is, the threshold, the fitting parameter a and b and the autoregressive constant, are optimized to fit with the distribution and the autocorrelation function of two model runs with high temporal resolution output that produced precipitation. The different precipitation classes rain, snow and graupel are summed up and downscaled together as one precipitation class. After the downscaling they are again split up according to their original fractions.

3.3.4. Cross correlations. The automatic rule search algorithm described in Section 3.2 has also been applied to search for possible cross correlations between the atmospheric downscaled variables. We found, for example, an overall cross correlation between wind speed and specific humidity of -0.27 (taking the whole database into account). Short- and long-wave radiation net fluxes are correlated by -0.52 in cloudy conditions, that is, if $CLC > 0$. These cross-correlations have been emulated in the noise-generating process

$$\epsilon'_{\psi} = \sqrt{(1 - |\sigma_{\text{cross}}|)}\epsilon_{\psi} + \sqrt{\sigma_{\text{cross}}}\epsilon_{\text{cross}}, \tag{10}$$

where ϵ_{ψ} is the noise term for a variable ψ in (6) and σ_{cross} is the respective cross correlation between two variables.

4. Results

In this section examples and statistics of the three steps of the downscaling approach are shown and discussed. The scheme has been tested for three case studies described in Section 2.2.2, that is, a calm sunny day, a convective showery day and a stratiform rainy day.

4.1. Case studies

The first downscaling step reduces already considerably the root mean square errors of the downscaled field for all variables, when compared to the coarse resolution field with the high-resolution model output as reference. A standard bi-linear interpolation algorithm using the four surrounding values, which has been tested for comparison only, does not lead to such a strong error reduction; here the errors are reduced only slightly, that is, the bi-quadratic spline interpolation leads to better results, see Table 5 (top). Moreover, a linear interpolation does not allow to conserve the coarse average to the same degree as the bi-quadratic interpolation (Table 5, bottom).

In Fig. 4 the results of the individual downscaling steps and the final results for a temperature field of the lowest atmospheric layer are shown. The coarse field (Fig. 4a) is smoothed by the average conserving splines (step 1, Fig. 4b). After calculating the temperature anomalies, using relief height as predictor (step 2, Fig. 4f) and adding these to the result from the first step (Fig. 4c), the still missing variance is estimated and added as spatially uncorrelated noise in step 3 (Fig. 4g). These three steps together add up to the final field (Fig. 4d), which resembles closely the original fine scale field (Fig. 4h). In this example the deterministic downscaling yields very good results, hence

Table 5. Root mean square errors of the coarse field, a high-resolution field obtained by the bi-quadratic spline interpolation (downscaling step 1) and for comparison a high-resolution field generated by a standard bi-linear interpolation spatially and temporally averaged for May 15, 2008. Top: RMSE for the small scale, bottom: RMSE for coarse scale.

Field	T (K)	FF ($\mathrm{m\,s^{-1}}$)	QV ($\mathrm{kg\,kg^{-1}}$)	PS (Pa)	S_{net}($\mathrm{W\,m^{-2}}$)	L_{net}($\mathrm{W\,m^{-2}}$)	PREC ($\mathrm{kg\,m^{-2}}$)
400 m scale							
Coarse	0.26	0.42	1.62e-04	282	20.2	4.36	2.10e-04
Bi-linear	0.24	0.40	1.47e-04	260	19.5	4.15	1.98e-04
Bi-quadratic	0.23	0.38	1.33e-04	236	18.3	3.91	1.75e-04
2.8 km scale							
Coarse	0	0	0	0	0	0	0
Bi-linear	0.10	0.13	6.2e-05	109	6.75	1.40	8.8e-05
Bi-quadratic	6.2e-04	9.4e-04	4.2e-07	0.75	0.05	0.01	6.2e-07

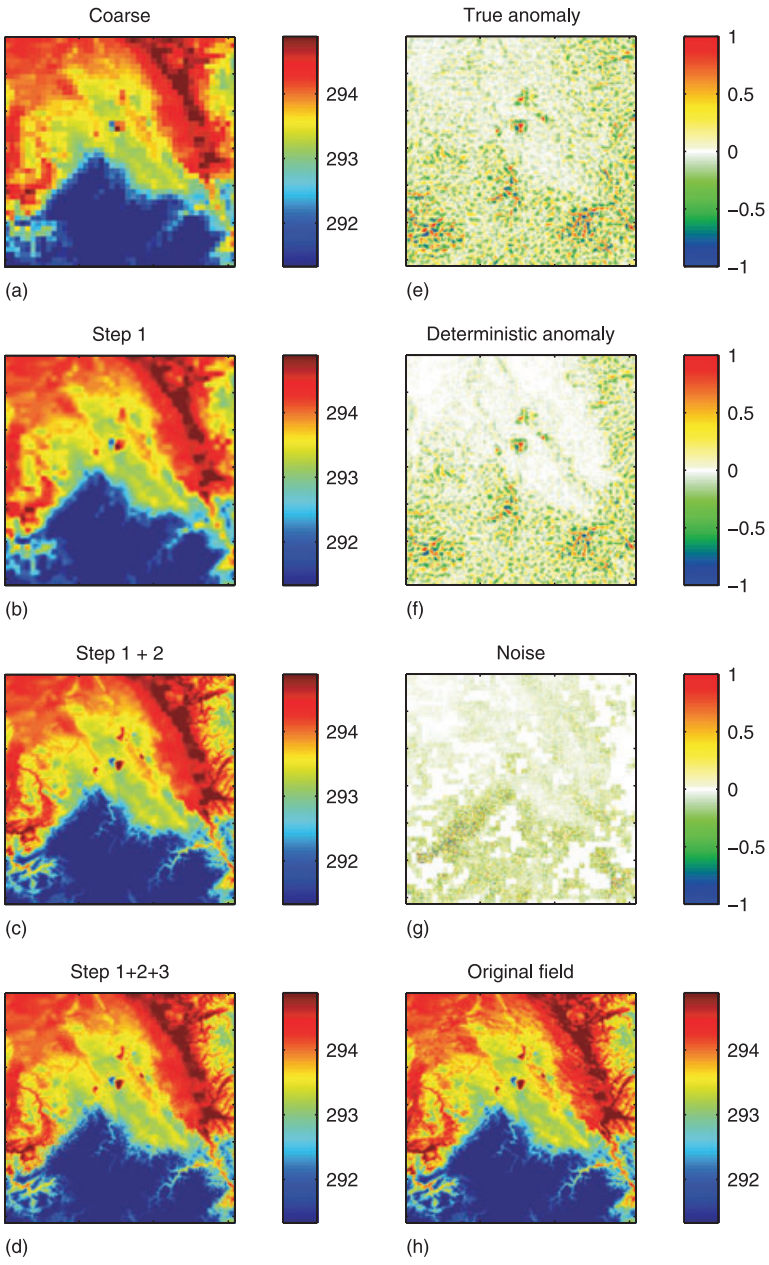

Fig. 4. Downscaling approach applied to a temperature field (in Kelvin) of the lowest atmospheric model layer, 10:00 UTC, May 12, 2008. (a) Coarse field; Field after application of (b) step 1 (spline interpolated); (c) step 1 + 2; (d) step 1 + 2 + 3 (final field, i.e. sum of all three downscaling steps); (e) true anomalies; (f) deterministic anomalies; (g) generated noise; (h) original fine scale field (reference).

the true anomalies (Fig. 4e) are well reproduced in downscaling step 2 (Fig. 4f). In contrast, in Fig. 5 a case is shown where the deterministic downscaling has less skill. During a clear cloudfree night, the air temperature does not decrease adiabatically with height, therefore the deterministic downscaling rule can only be applied to a very small part of the model domain (Fig. 5a). Thus the main part of the subgrid scale variability is generated by the noise step (Fig. 5b). Since the spatial subgrid scale correlations are not modelled, the spatial characteristics of the true anomalies (Fig. 5c) are not well reconstructed. In the original field cold air gathers in some of the valleys, which cannot be recovered by a simple statistical method.

Figure 6 shows an example for the downscaling of long-wave net radiation at the surface. We start again from the coarse field (Fig. 6a), apply the spline interpolation (Fig. 6b), and add the deterministic anomaly proportional to the surface temperature anomalies, which leads to the intermediate field Fig. 6c. The addition of noise (step 3) finally leads to Figure 6d. In the original field (Fig. 6e and h) a small region in the northeastern part shows particular large small-scale variability. This large scatter is not reconstructed in step 2 (see Fig. 6f), because this variability is not caused by surface heterogeneity but by some sparse clouds. The missing variance is satisfactorily replenished by step 3 (Fig. 6g).

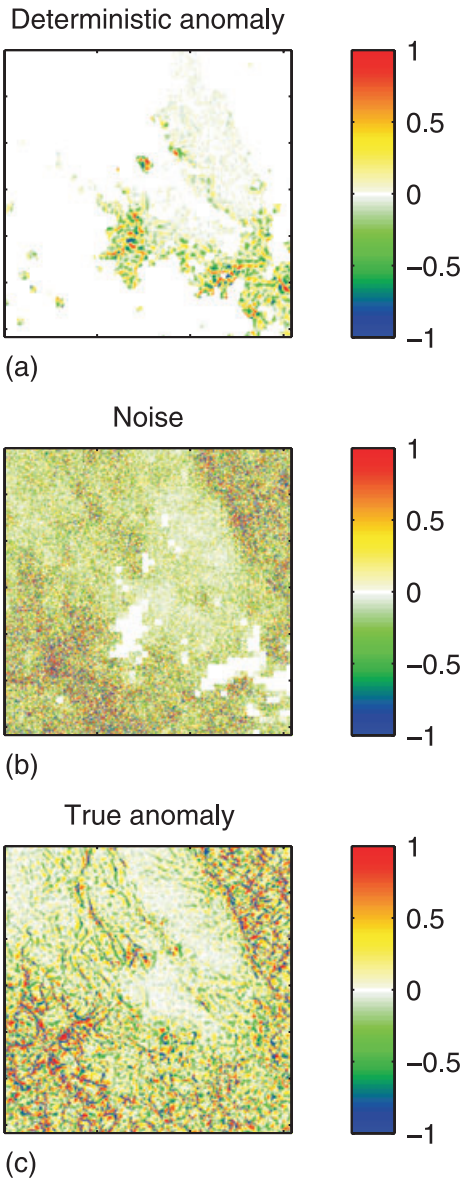

Fig. 5. Temperature anomalies (in Kelvin) constructed in downscaling step 2 (a) and downscaling step 3 (b) and reference anomalies for a clear-sky nighttime situation, 1:00 UTC, May 12, 2008.

The time series of the root mean square errors (RMSE) produced by the individual downscaling steps is shown in Fig. 7 for a case study of May 12, 2008. The first step (spline interpolation) leads for all variables to a small error reduction compared to the coarse fields (here the error of the coarse field at the small scale is computed by assuming homogeneous forcing for all subpixels). Where applicable, that is, for temperature, pressure and the radiation fluxes, the deterministic downscaling leads to a considerable error reduction. The error reduction for temperature (Fig. 7a) during the clear sky night is less distinctive than during the day. These problems do not exist during overcast nights (not shown). Adding random noise in the third step naturally increases the RMSE error again for most variables (temperature at night, humidity, wind speed and the radiation fluxes in the evening, in this case); sometimes the RMSE even exceeds the RMSE caused by the homogeneous field.

As mentioned above, the correct subgrid scale variability is decisive to avoid biases for applications involving non-linear processes. The first downscaling step introduces some variance (see Fig. 8) compared to the coarse values, which have no subgrid scale variance at all. The second step leads to a another large increase of the high-resolution standard deviation. Even more subgrid variability is generated by step 3, in which the still missing variance is estimated and added. The subgrid heterogeneity is well parametrized, but temporary deviations from the reference do occur. For pressure the third step is not applied because the variability generated in the second downscaling step is already sufficient (see Fig. 8d).

For comparison the root mean square errors and subgrid scale standard deviations for May 15, 2008, a convective showery day, are depicted in Fig. 9. Results are shown only for those variables which exhibit a different behaviour compared to the calm, sunny day in the previous example. Here for the radiation fluxes almost no improvements can be achieved by the second downscaling step, because the subgrid scale variability is dominated by the heterogeneous cloud cover. The subgrid scale standard deviation of the precipitation is reproduced well for this day (Fig. 9d).

The errors and subgrid scale variabilities are averaged spatially and temporally for the three case studies and listed in Tables 6 and 7. According to these results the errors are reduced slightly by the first downscaling step and strongly by the second downscaling step. The overall improvement gained for the radiation fluxes is less than for the single fair weather day shown in Fig. 7, because for the two other cloudy days the deterministic downscaling step has much less skill. Only under clear sky conditions the RMSE is reduced considerably by the second downscaling step, otherwise the subgrid scale variability is not due to surface heterogeneity but to variable cloud cover. The subgrid scale variability is enhanced slightly by downscaling step 1 and more by step 2 (where applicable) and step 3 (Tab. 7). For all variables the subgrid standard deviation is on the average slightly too large after the last step, but only the deviations for wind speed, pressure and long-wave net radiation are statistically significant. Obviously the mean statistics of these three days do not match the mean statistics of the training data set.

The temporal autocorrelations of the coarse fields are larger than the reference values from the high-resolution fields (see Fig. 10), this difference prevails after step 1 and 2. Step 3 leads to a strong decrease of the autocorrelations with increasing time lags; for most variables the reference autocorrelations are now matched more closely. For precipitation the correlations are, however, too low after the third step.

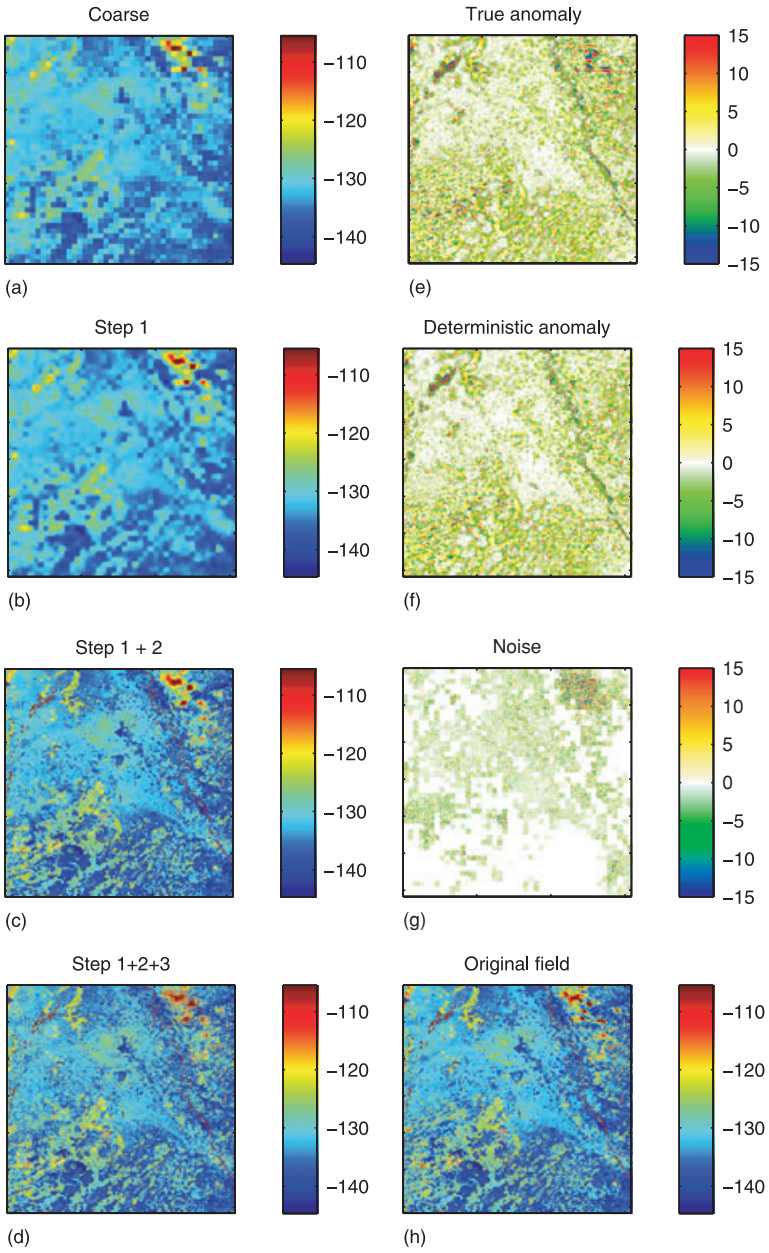

Fig. 6. Same as Fig. 4, but for the long-wave surface net radiation in W m^{-2}.

5. Discussion and conclusions

A downscaling system for atmospheric near-surface variables has been developed. Possible applications are the generation of high-resolution input for SVAT models and hydrological models, based on low-resolution atmospheric model output. The scheme can be employed for stand-alone applications or in a fully coupled (climate) model system.

The downscaling approach consists of three steps. In a first step, an average-conserving bi-quadratic spline interpolation is carried out, in a second step physical relationships with surface properties are exploited by linear regression wherever possible. Automatically derived rules indicate whether a regression with a surface quantity as predictor is applicable, because not all relationships found are usable under all atmospheric conditions. Useful correlations with surface variables were found for temperature, pressure and the radiation fluxes, but not for specific humidity, wind speed and precipitation. In the third step the missing small-scale variability is estimated and added as autoregressive noise.

The approach has been tested by applying it to the variables of the lowest model layer of the COSMO model for three case studies with different weather situations. Using the high-resolution COSMO-model output as reference, we found that the first two

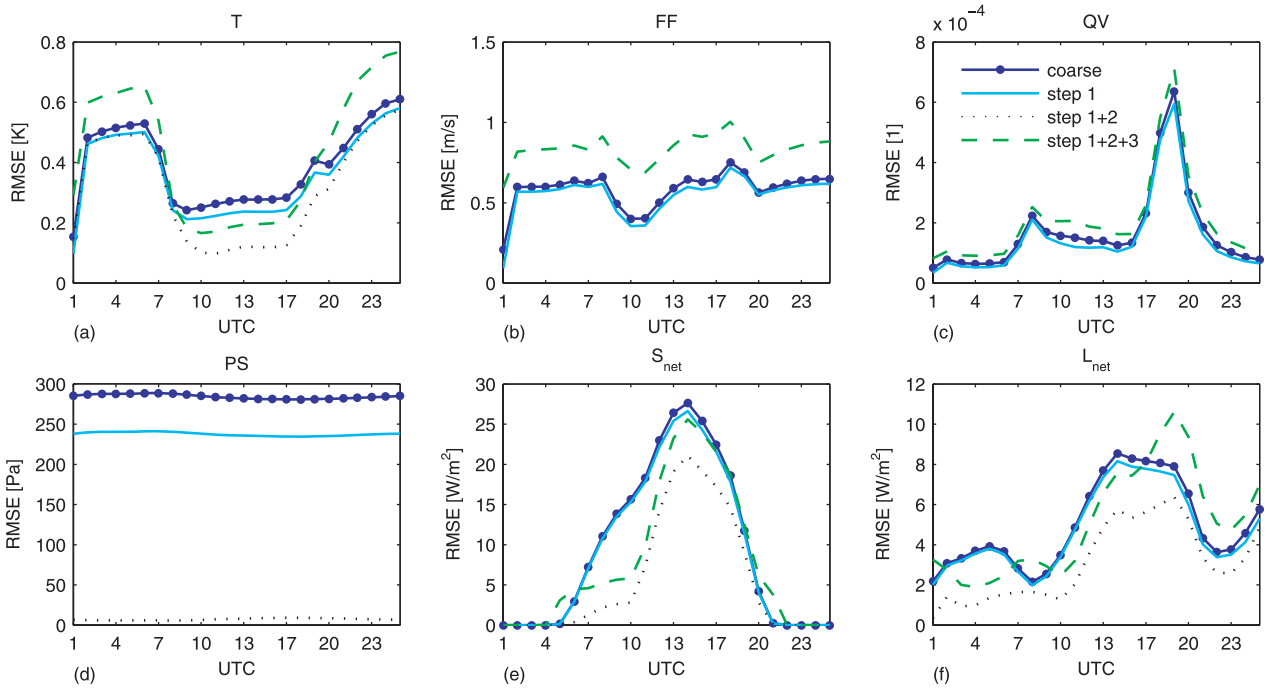

Fig. 7. Time series of root mean square error (RMSE) of the downscaling variables for the three downscaling steps for May 12, 2008: (a) temperature, (b) wind speed, (c) specific humidity, (d) surface pressure, (e) short-wave net radiation, (f) long-wave net radiation. For wind speed, specific humidity and precipitation the deterministic step 2 is not applicable, see Section 3.2.

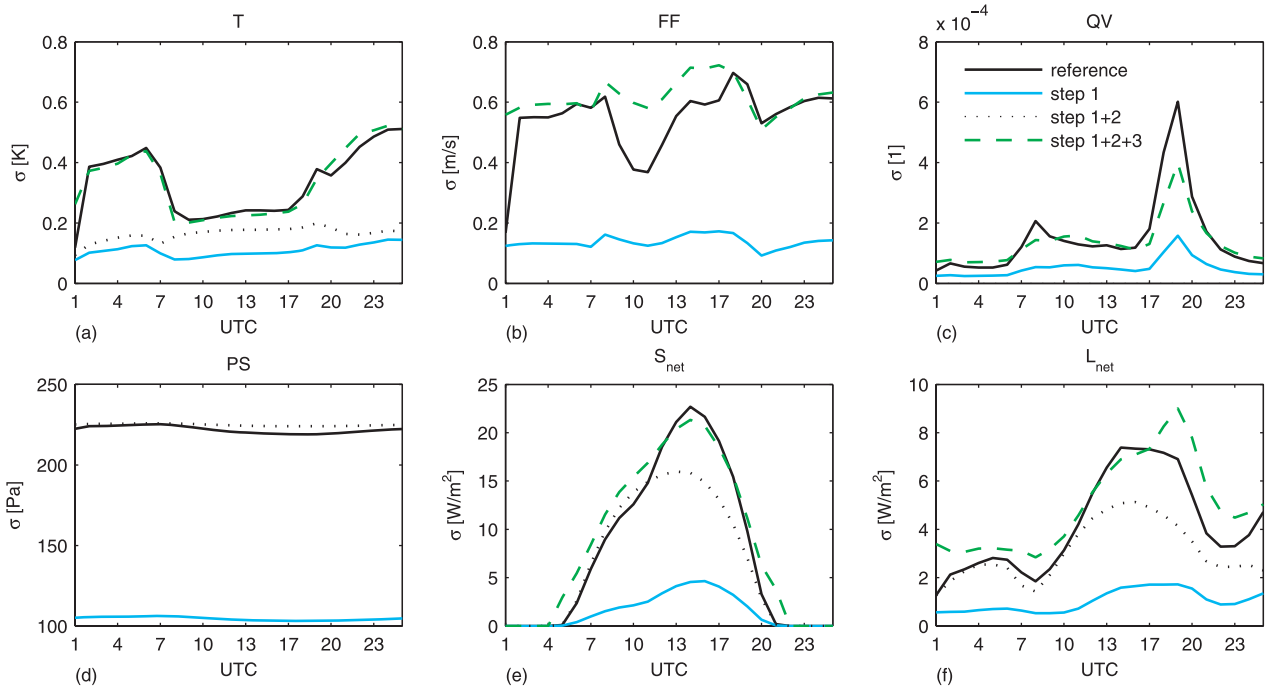

Fig. 8. The same as Fig. 7 for the subgrid scale standard deviations (σ). Here the black line denotes the reference subgrid standard deviations.

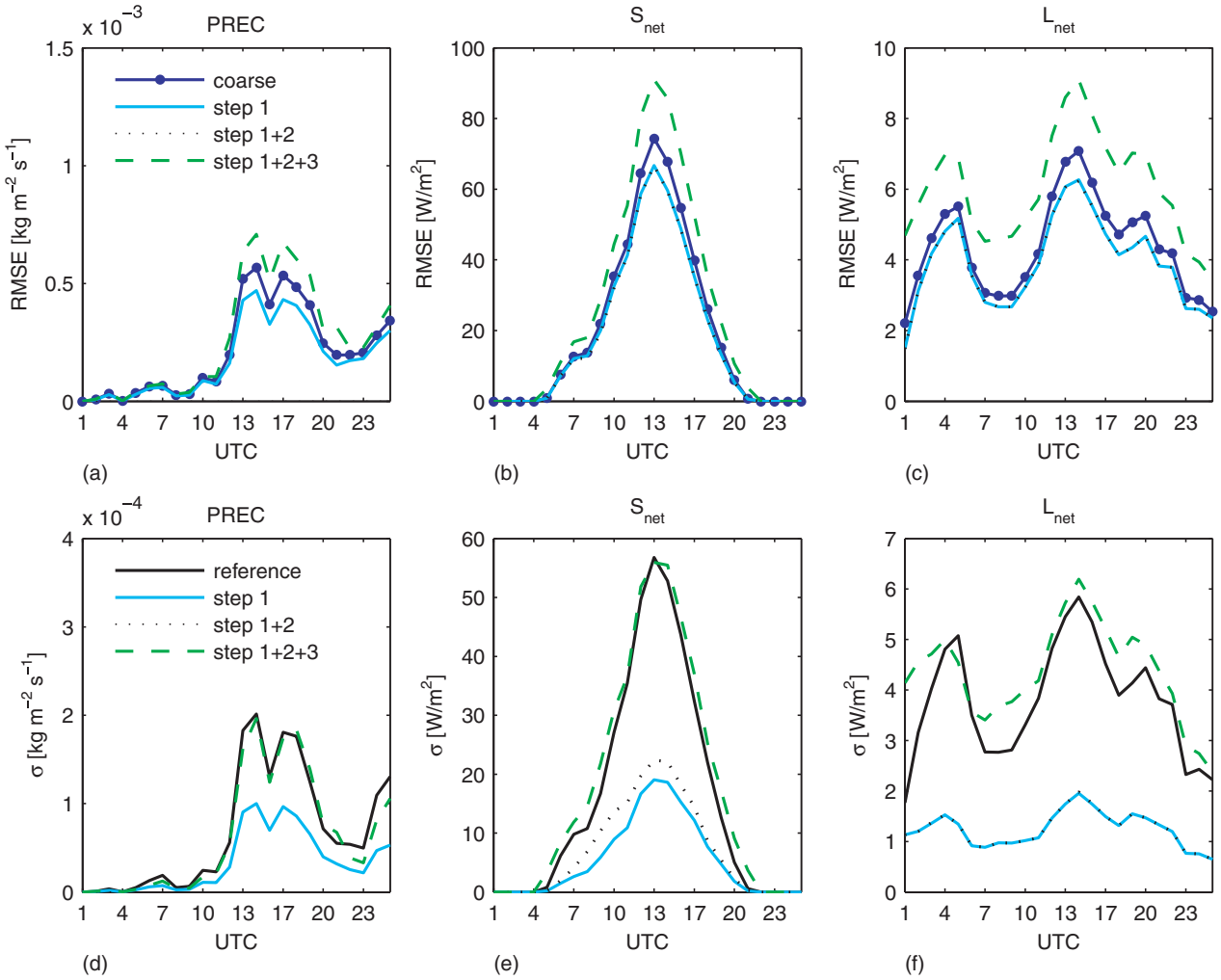

Fig. 9. Top panel: root mean square errors for short- and long-wave radiation fluxes and precipitation for May 15, 2008. Bottom panel: the respective subgrid scale variances.

Table 6. Root mean square errors for the different variables for the downscaling steps averaged over the three case studies

Disaggregation	T (K)	FF (m s^{-1})	QV (kg kg^{-1})	PS (Pa)	S_{net}(W m^{-2})	L_{net}(W m^{-2})	PREC (kg m^{-2})
No disagg	0.31	0.56	1.54e-04	285	14.73	5.09	7.75e-05
Step 1	0.27	0.52	1.34e-04	238	13.52	4.70	6.49e-05
Step 1+2	0.21	–	–	6.2	12.18	4.15	–
Step 1+2+3	0.31	0.82	1.94e-04	–	17.97	6.26	9.92e-05

Table 7. Subgrid standard deviations for the different variables for downscaling steps averaged over the three case studies

Disaggregation	T (K)	FF (m s^{-1})	QV (kg kg^{-1})	PS (Pa)	S_{net}(W m^{-2})	L_{net}(W m^{-2})	PREC (kg m^{-2})
Step 1	0.10	0.13	5.19e-05	105	3.52	1.23	1.16e-05
Step 1+2	0.17	–	–	225	6.03	1.94	–
Step 1+2+3	0.28	0.61	1.36e-04	–	13.37	4.72	2.50e-05
Reference	0.27	0.52	1.35e-04	222	11.57	4.25	2.53e-05

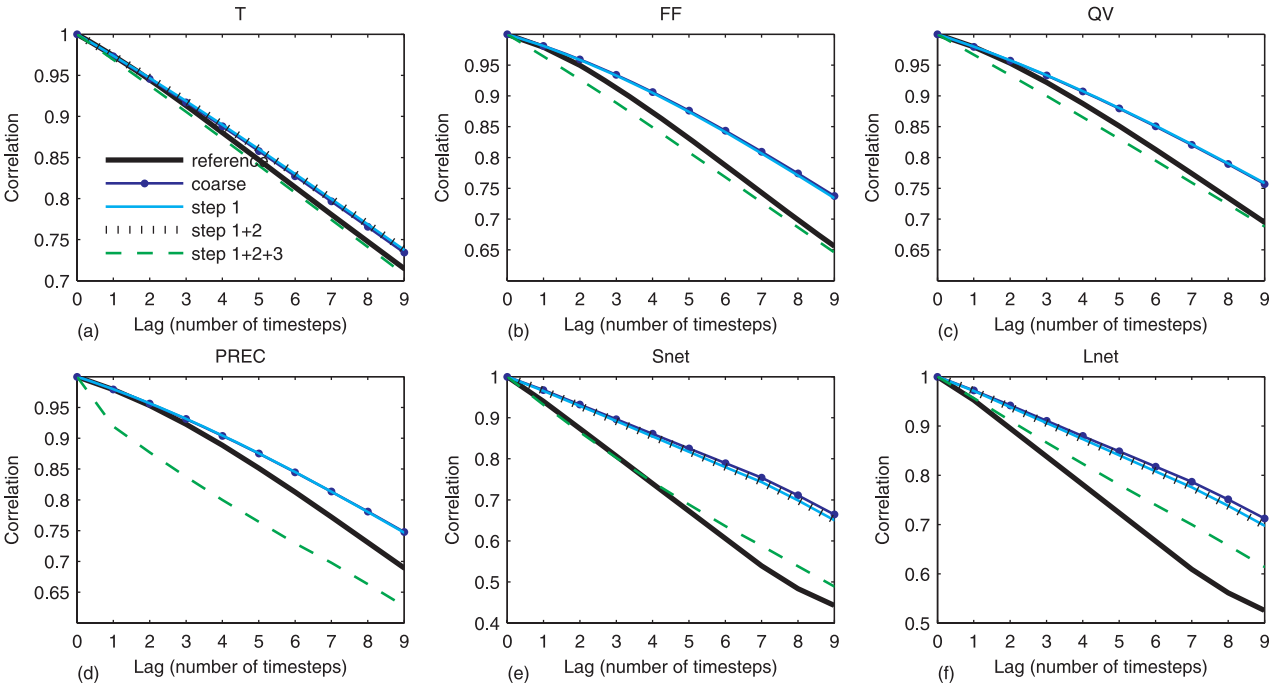

Fig. 10. Temporal autocorrelations for the downscaling variables for 17:00 UTC, May 15, 2008. Here one time step is 24 s.

downscaling steps considerably reduce the errors compared to the homogeneous coarse scale values. All steps increase the subgrid scale variance towards the reference small-scale variability. The first step leads to a small error reduction and a small increase of the subgrid scale variability. The second step, wherever applicable, largely reduced the errors and adds some variability. Since step 2 is weather dependent also the performance of the disaggregation is dependent on the atmospheric conditions. The third step achieves a good reproduction of the subgrid scale variability, however, at the expense of an increased root mean square error. This was also the case in a study by Venema et al. (2009), who developed a downscaling scheme for 3-D-cloud fields, which increased the root mean square errors of liquid water content on the small scale. They showed, however, that the errors in radiation fluxes based on radiative transfer calculations made with the downscaled fields as input led to a considerable error decrease. This outcome results from the non-linear processes in radiative transfer, where the correct simulation of subgrid scale statistics is of crucial importance. Thus, when employing the downscaling system, it should be decided first whether the lowest possible errors or a realistic small-scale variability is more important.

The question remains whether the weak correlations of near surface wind speed and specific humidity with surface variables is a model-specific behaviour, or whether this is also valid for other models and for measurements. Bertoldi et al. (2008) for example coupled a large-eddy simulation (LES) model to a surface energy balance scheme and found strong correlations of the near-surface atmospheric properties with surface variables. In their study near-surface atmospheric temperature was strongly correlated with the sensible heat flux, specific humidity with the latent heat flux, and the wind speed with surface roughness. They looked at scales of $L = 10^1$ to 10^3 m, which are similar to the scales considered in this study. They found the strongest correlations between surface and atmospheric quantities to be one pixel downwind the respective surface pixel. Spatial lags have not yet been considered in this study. Another difference is the vertical resolution, the lowest atmospheric model level in the LES used by Bertoldi et al. (2008) is in 2.5 m height, compared to 10 m in our case. The different correlations found may also be due to different transfer parametrizations for the turbulent exchange fluxes in their coupling and in the COSMO model.

In this study, we have developed and tested a downscaling system for atmospheric variables based on 400 m grid spacing as the smaller scale and 2.8 km as the larger scale. First tests of the system for a downscaling from 14 km data down to 2.8 km have been conducted in order to see whether the system can also be used for regional climate simulations with the COSMO model on a 14 km grid, with surface information on a 2.8 km mosaic. Although the downscaling steps have been trained for smaller scales, the results obtained by the downscaling are very encouraging in terms of root mean square error reduction and subgrid scale variance reconstruction. These results indicate that the approach could also be employed in the field of climate modelling. Using a mosaic approach for the soil and surface processes with the downscaling system presented in this paper as coupling between the two scales could lead to a better, less biased simulation of the energy and water budget

of the lower atmospheric boundary and thus to better climate simulations.

In the future we will try to conserve also spatial correlations in downscaling step 3, that is, to generate red noise instead of white noise. This would be important for distributed hydrological models in contrast to most SVAT models, which are usually one-dimensional single-column-models and do not simulate lateral exchange.

The downscaling system is applicable whenever a mosaic approach is used in an atmospheric model. In the so-called tile approach (see for example Avissar and Pielke, 1989; Avissar, 1991; Heinemann and Kerschgens, 2005; Ament and Simmer, 2006) the soil processes are modelled separately for different land use classes, available at the subgrid scale, and the resulting fluxes are averaged according to the fractional coverage of these land use classes. Hence, in the tile approach only one

Table A1. Possible predictors (available on high resolution) and indicators (coarse resolution) for the deterministic downscaling. The predictors gradients × orography are computed by using the coarse temperature gradient information (because fine scale information is usually not available) and the fine scale surface information on the relief height

	Possible predictors		Possible indicators
T_g	Ground temperature (K)	$Tgr25$	Temperature gradient of lowest two layers (25 m) [K m^{-1}]
H	Orography (m)	$Tgr60$	Temperature gradient of lowest three layers (60 m) [K m^{-1}]
LAI	Leaf area index (1)	$Tgr105$	Temperature gradient of lowest four layers (105 m) [K m^{-1}]
$z0$	Roughness length (m)	$QVgr25$	Specific humidity gradient of lowest two layers (25 m) [m^{-1}]
$ln(z/z0)$	Logarithmic roughness ratio between height of lowest model layer and roughness length (1)	$QVgr60$	Specific humidity gradient of lowest three layers (60 m) [m^{-1}]
QVS	Specific humidity at surface (kg kg^{-1})	$QVgr105$	Specific humidity gradient of lowest four layers (105 m) [m^{-1}]
$Tgr25 \times H$	Temperature gradient of lowest two layers (25 m) × orography (K)	θ	Cosine of solar zenith angle [1]
$Tgr60 \times H$	Temperature gradient of lowest three layers (60 m) × orography (K)	LWP	Liquid water path [kg m^{-2}]
$Tgr105 \times H$	Temperature gradient of lowest four layers (105 m) × orography (K)	LWP_{var}	LWP variance of 3 × 3 coarse pixels [kg^2 m^{-4}]
$QVgr25 \times H$	Specific humidity gradient of lowest two layers (25 m) × orography (1)	ORO_{var}	Orography variance of 3 × 3 coarse pixels [m^2]
$QVgr60 \times H$	Specific humidity gradient of lowest three layers (60 m) × orography (1)	FF	Wind speed [m s^{-1}]
$QVgr105 \times H$	Specific humidity gradient of lowest four layers (105 m) × orography (1)	DD	Wind direction (°)
$SHFL$	Sensible heat flux (W m^{-2})	U	Near-surface u-wind component (m s^{-1})
$LHFL$	Latent heat flux (W m^{-2})	V	Near-surface v-wind component (m s^{-1})
FR_{land}	Fraction of land (1)	CLC	Cloud cover (%)
W_{so}	Soil moisture of top soil layer (m H_2O)	CLC_{var}	Cloud cover variance of 3 × 3 coarse neighbouring pixels (%)
		QV	Near-surface specific humidity (1)
		RH	Near-surface relative humidity (1)
		QVS_{var}	Variance of 3 × 3 neighbouring pixels of surface specific humidity (1)
		S_{net}	Short-wave net radiation at surface (W m^{-2})
		L_{net}	Long-wave net radiation at surface (W m^{-2})
		PS	Surface pressure (Pa)
		$PREC$	Precipitation [kg m^{-2} s^{-1}]
		FR_{land}	Fraction of land (1)

source of subgrid heterogeneity is accounted for; this is usually the land use, while topographic or soil texture variability is not considered. The approach presented here can not be applied without modifications to such a tiled surface, because high-resolution surface information of different surface properties is necessary, for example of topographic height, albedo and surface temperature, which usually is available in a consistent way only in the explicit subgrid mosaic approach.

In an upcoming paper the downscaling system will be implemented into the COSMO-model and the impact on the simulation of the turbulent heat fluxes and the overall model performance will be evaluated.

6. Acknowledgments

We gratefully acknowledge financial support by the SFB/TR 32 Patterns in Soil–Vegetation–Atmosphere Systems: Monitoring, Modelling, and Data Assimilation funded by the Deutsche Forschungsgemeinschaft (DFG), in which framework this work has been carried out. We thank Guido Waldhoff for the support in acquiring and preparing the surface data. Moreover, we thank the German Meteorological Service (DWD) for the access to the COSMO-analyses data archive and the COSMO model code. The structure of this paper has benefited notably thanks to the comments of two anonymous reviewers.

7. Appendix: details of the downscaling system

Table A1 contains all predictors and indicators provided to the automatic rule search system described in Section 3.2, the rules that were found are given in Table A2. The complete regression equations for the subgrid scale standard deviations are

$$\begin{aligned}
\sigma_T &= 4.3255 \times Tgr25 + 0.5026 \times \sigma_c^{3\times3} \\
&\quad - 1.5497 \times 10^{-5} \times PS + 1.6125 \\
\sigma_{FF} &= 0.7762 \times \sigma_c^{3\times3} - 4.2692 \times 10^{-5} \times PS + 4.5029 \\
\sigma_{QV} &= 0.7076 \times \sigma_c^{3\times3} + 1.2202 \times 10^{-5} \\
\sigma_{S_{\text{net}}} &= 0.8882 \times \sigma_c^{3\times3} + 4.2606 \\
\sigma_{L_{\text{net}}} &= 0.7 \times \sigma_c^{3\times3} + \sigma_{\text{qvs}}.
\end{aligned}$$

Table A2. Deterministic downscaling rules found by the automatic rule search algorithm. Shown are relationships between the downscaling variables, i.e. the predictands, and possible predictors for indicators above or below a certain threshold of the indicator value. At least a correlation above 0.7 between predictor and predictand was necessary, and at least 10% of all cases of the data set needs to be covered by this rule. For abbreviations of the variables see Tables 2 and A1

Predictand	Predictor	Indicator with threshold	Correlation	Data coverage (%)
$\boldsymbol{T}$	$Tgr105 * H$	$Tgr105 < 0.0022$	0.74	59
		$Tgr60 < 0.0037$	0.75	58
		$Tgr25 > 0.0065$	0.75	56
		$FF > 5.1$	0.71	12
		$LWP > 0.095$	0.71	10
		$U > 3.2$	0.71	17
		$S_{\text{net}} > 204$	0.81	29
	$Tgr60 * H$	$Tgr105 < 0.0022$	0.71	59
		$Tgr60 < 0.0037$	0.74	58
		$Tgr25 < 0.0065$	0.76	56
		$U > 3.7$	0.78	13
		$S_{\text{net}} > 204$	0.81	29
	$Tgr25 * H$	$Tgr105 < -0.0048$	0.82	47
		$Tgr60 < -0.00155$	0.78	52
		$Tgr25 < 0.0065$	0.72	56
		$S_{\text{net}} > 204$	0.78	29
	H	$Tgr105 < 0.0058$	−0.74	64
		$Tgr60 < 0.0090$	−0.73	64
		$Tgr25 > 0.0161$	−0.72	63
		$\Theta > 0.82$	−0.7	17
		$FF > 4.0$	−0.76	23
		$LWP > 0.095$	−0.78	10
		$U > 3.2$	−0.78	17
		$S_{\text{net}} > 179$	−0.72	31
		$L_{\text{net}} > -15.224$	−0.7	17
$\boldsymbol{L_{\text{net}}}$	T_g	$clc < 43$	−0.72	38
		$L_{\text{net}} < -82.5$	−0.74	36

$\sigma_c^{3\times3}$ is the standard deviation of the respective variable of the 3×3 surrounding grid boxes, and σ_{qvs} is the subgrid scale standard deviation of surface specific humidity.

References

Ament, F. and Simmer, C. 2006. Improved representation of land-surface heterogeneity in a non-hydrostatic numerical weather prediction model. *Bound. Layer Meteorol.* **121**(1), 153–174.

Arola, A. 1999. Parameterization of turbulent and mesoscale fluxes for heterogeneous surfaces. *J. Atmos. Sci.* **56**, 584–598.

Avissar, R. 1991. A statistical-dynamical approach to parameterize subgrid-scale land-surface heterogeneity in climate models. *Surv. Geophys.* **12**, 155–178.

Avissar, R. and Pielke, R. A. 1989. A parameterization of heterogeneous land surfaces for atmospheric numerical models and its impact on regional meteorology. *Mon. Wea. Rev.* **117**, 2113–2136.

Bachner, S., Kapala, A. and Simmer, C. 2008. Evaluation of daily precipitation characteristics in the CLM and their sensitivity to parameterizations. *Meteorol. Z.* **17**(13), 407–419.

Baldauf, M., Förstner, J., Klink, S., Reinhardt, T., Schraff, C. and co-authors. 2009. Kurze Beschreibung des Lokal-Modells Kürzesfrist COSMO-DE (LMK) und seiner Datenbanken auf dem Datenserver des DWD. Deutscher Wetterdienst, Geschäftsbereich Forschung und Entwicklung, Offenbach, Germany.

Bertoldi, G., Kustas, W. P. and Albertson, J. D. 2008. Estimating spatial variability in atmospheric properties over remotely sensed land surface conditions. *J. Appl. Meteor. Climatol.* **47**, 2147–2165.

Boé, J., Terray, F., Habets, F. and Martin, E. 2007. Statistical and dynamical downscaling of the Seine basin climate for hydro-meteorological studies. *Int. J. Clim.* **27**, 1643–1655.

Böhm, U., Kücken, M., Ahrens, W., Block, A., Hauffe, D. and co-authors. 2006. CLM—the Climate Version of LM: Brief description and long-term applications. Consortium of Small-Scale Modelling (COSMO)—Newsletter No. 6, Deutscher Wetterdienst, Geschäftsbereich Forschung und Entwicklung, Offenbach, Germany, 225–235.

Dickinson, R., Henderson-Sellers, A. and Kennedy, P. 1993. Biosphere Atmosphere Transfer Scheme (BATS) version 1e as coupled to the NCAR Community Climate Model. NCAR Tech. Note NCAR/TN-387-STR, Natl. Cent. for Atmos. Res. Boulder Colorado.

Doms, G., Förstner, J., Heise, E., Herzog, H.-J., Raschendorfer, M. and co-authors. 2007. A description of the nonhydrostatic regional model LM. Part II: physical parameterization. Deutscher Wetterdienst, P.O. Box 100465, 63004 Offenbach, Germany.

EEA, Corine Land Cover (CLC90) 2000. European Environment Agency, http://dataservice.eea.eu.int/dataservice/, Copenhagen, DK.

Farr, T. G., Rosen, P. A., Caro, E., Crippen, R., Duren, R. and co-authors. 2007. The shuttle radar topography mission. *Rev. Geophys.* **45**, doi:10.1029/2005RG000183.

Giorgi, F., Francisco, R. and Pal, J. 2003. Effects of a subgrid-scale topography and land use scheme on the simulation of surface climate and hydrology. Part I: effects of temperature and water disaggregation. *J. Hydrol.* **4**(Part 2), 317–333.

Heinemann, G. and Kerschgens, M. 2005. Comparison of methods for area-averaging surface energy fluxes over heterogeneous land surfaces using high-resolution non-hydrostatic simulations. *Int. J. Clim.* **25**, 379–403.

Naden, P. S. 1992. Spatial variability in flood estimation for large catchments: the exploitation of channel network structure, *Hydrol. Sci.* **37**(1), 53–71.

Schlünzen, K. H. and Katzfey, J. J. 2003. Relevance of sub-grid-scale land-use effects for mesoscale models, *Tellus*, **55A**, 232–246.

Seth, A. and Giorgi, F. 1994. Simulating fluxes from heterogeneous land surfaces: explicit subgrid method employing the biosphere-atmosphere transfer scheme (BATS), *J. Geophys. Res.* **99**(D9), 18 651–18 667.

Seuffert, G, Gross, P., Simmer, C. and Wood, E. F. 2002. The influence of hydrologic modeling on the predicted local weather: two-way coupling of a mesoscale weather prediction model and a land surface hydrologic model, *J. Hydromet.* **3**(5), 505–523.

Singh, V. P. 1997. Effect of spatial and temporal variability in rainfall and watershed characteristics on stream flow hydrograph, *Hydrol. Process.* **11**, 1649–1669.

Smagorinsky, J. 1963. General circulation experiments with the primitive equations: 1. The basic experiment, *Mon. Wea. Rev.* **91**, 99–164.

Steppeler, J., Doms, G., Schättler, U., Bitzer, H., Gassmann, A. and co-authors. 2003. Meso-gamma scale forecasts using the non-hydrostatic model LM, *Meteor. Atmos. Phys.* **82**, 75–96.

Venema, V., Garcia, S. G. and Simmer, C. 2010. A new algorithm for the downscaling of 3-dimensional cloud fields, *Q. J. R. Meteorol. Soc.* **136**, 91–106, doi:10.1002/qj.535.